Electronic Supplementary Information

Evolving Mineralogy and Reactivity of Hematite-Coated Sands During Reduction of 4-Chloronitrobenzene by Fe(II) in Flow-Through Reactors

Celina M. Harris[†], Adel Soroush[‡], Alanna M. Hildebrandt[†], Kamilah Y. Amen[†], Louis G. Corcoran[†], Joshua M. Feinberg[§], William A. Arnold[‡,*], and R. Lee Penn[†,*]

[†] Department of Chemistry, University of Minnesota – Twin Cities, Smith Hall, Pleasant St SE, Minneapolis, MN 55455, USA
[‡] Department of Civil, Environmental, and Geo- Engineering, University of Minnesota – Twin Cities, 500 Pillsbury Drive SE, Minneapolis, Minnesota 55455, USA
[§]Institute for Rock Magnetism and Department of Earth & Environmental Sciences, University of Minnesota, Minneapolis, Minnesota 55455, USA

*Authors to whom correspondence should be addressed.
R. Lee Penn Phone: (612) 626-4680 Fax:1 (612) 626 7541 email: rleepenn@umn.edu
William A. Arnold Phone: 612-625-8582; Fax: 612-626-7750; email: arnol032@umn.edu

Environmental Science: Nano

S1. Additional Materials and Methods

S1.1 Chemical Sources and Purities

Sodium chloride (ACS reagent grade) was purchased from Mallinckrodt. Sodium bicarbonate (99.7%) was purchased from Sigma-Aldrich and solutions were prepared with deoxygenated ultrapure water under anaerobic conditions. Iron (II) chloride tetrahydrate (≥ 99%) and Fe (III) nitrate nonahydrate (ACS reagent grade) were purchased from Fisher Scientific. Iron (II) chloride tetrahydrate solids and solutions were stored and prepared under anaerobic conditions. 3-(2-pyridyl)-5,6-diphenyl-1,2,4-triazine-p_2p'-disulfonic acid monosodium salt hydrate, (ferrozine, 97%), acetonitrile (HPLC grade), ammonium acetate (97%), methanol (HPLC grade), nitric acid (15.8 M), and water (HPLC grade) were purchased from Sigma-Aldrich. Hydrochloric acid (BDH Aristar, 12.1 M) and NaOH (Fisher Scientific, 19 M) were used to make solutions for pH adjustments. 4-Chloronitrobenzene (4-ClNB; ≥ 98%) and 4-chloroaniline (4-ClAn; ≥ 98%) were purchased from Acros Organics. Stock solutions of 4-ClNB and 4-ClAn were prepared at 60 mM in deoxygenated methanol under anaerobic conditions. Stock solutions were further diluted to 10 mM and 0.1 mM in ultrapure deoxygenated water. The 0.1 mM stock solutions were used to prepare the HPLC standards. The 60 mM stock of 4-chloronitrobenzene was used for preparation of the 0.1 mM 4-ClNB in 10 mM $NaHCO_3$.

S1.2 Column Hydrodynamic Characterization

To characterize column properties, chloride ion concentration plotted against eluted volume enabled calculation of a pore volume, which was identified as the point where $C/C_0 = 0.5$ based on fitting with a sigmoidal Boltzmann function with an iterative Levenberg-Marquart algorithm in Origin Lab 2019. All subsequent plots were prepared as concentration versus pore volume by dividing the eluted volume by the initial pore volume. Plots of C/C_0 for chloride versus pore volume were subsequently fit to the solution of the one-dimensional advection-dispersion equation for a step input initial condition and semi-finite boundary condition:[1]

$$\frac{C}{C_0} = \frac{1}{2} erf\left(\frac{(R-T)}{\sqrt{\frac{4T}{Pe}}}\right) + \frac{1}{2} e^{Pe} erf\left(\frac{(R+T)}{\sqrt{\frac{4T}{Pe}}}\right) \quad \text{(S1)}$$

where T is the number of pore volumes, Pe is the Peclet number, and R is the retardation coefficient to account for linear and reversible sorption. For a conservative tracer, such as NaCl, R should be approximately unity.

Nonlinear curve fitting was performed using Origin Lab 2019 to obtain Pe and R. Additional calculations were performed to determine the porosity (ε, equation S2) and hydrodynamic dispersion coefficient (D, equation S3) of the column before and after the reaction.

$$\varepsilon\varepsilon = \frac{T_1}{AL} \tag{S2}$$

$$D = \frac{QQL}{A\varepsilon\varepsilon Pe} \tag{S3}$$

Porosity was determined based on the volume of solution needed to achieve one pore volume (T_1), cross-sectional area of the column (A), and length of the column (L). The hydrodynamic dispersion coefficient was determined from the flow rate (Q), length of the column, cross-sectional area, porosity, and Peclet number.

S1.3 Sorption capacity of high coverage (HFe) sand

Fe(II) adsorption on hematite-coated sand was quantified in an anaerobic glovebag (Coy Laboratory Products) with a 5% H_2, 95% N_2 (Airgas) atmosphere. The pH of the solutions was adjusted to 7.0 ± 0.5 using 1 M HCl and 1 M NaOH. Reactors were crimp-capped with Teflon lined aluminum caps and equilibrated with end-over-end rotation for 21 hours. Following equilibration, the pH of each solution was measured. Supernatants from the serum bottles were filtered using 13 mm syringe filters with a 0.2 μm nylon membrane (PALL Life Sciences Acrodisc) before analysis.

The absorbed concentration was determined from the difference between the initial and final aqueous concentrations. The quantity of Fe(II) sorbed per gram of sand and the final aqueous Fe(II) concentration were fitted to the Langmuir sorption model:

$$\chi\chi = \frac{\chi\chi_{max}\kappa_L\mathcal{C}}{1 + K_L C} \tag{S4}$$

where X is the amount of Fe(II) adsorbed per mass of sand (μg/g), C is equilibrium Fe(II) concentration (μg/L), X_{max} is the maximum adsorption capacity (μg/g), and K_L is a binding constant (L/μg).

For the HFe sand, Fe(II) sorption capacity was determined at pH 7 and the data fit to a Langmuir sorption model (Fig. S1). The maximum sorption capacity was reached at 51 ±1 μg Fe(II) per gram of sand, which translates to approximately 120 μg Fe(II) per mg of hematite. This number is significantly higher than the maximal surface coverage of Fe(II) that could be achieved, as determined from the surface area for the hematite particles[2] and the divalent metal site capacity of hematite,[3] of approximately 20 μg Fe(II) per mg of hematite. Previous work, using similar experimental conditions, has shown that the sorption capacity of the Ottawa sand standard is 68 ± 2 μg Fe(II) per gram of sand. This value, being slightly higher than the capacity for the HFe sand, suggests that the aqueous Fe(II) is sorbing to both the hematite and sand surfaces. Given the similarity between the sorption capacities for the HFe sand and the sand standard, and the intermediate hematite coverage for the LFe sand in comparison to the former two samples, Fe(II) sorption capacity for LFe sand was not determined.

S1.4 Iron Oxide Detachment (ineffective)

To detach hematite from the sand, approximately 4 g of coated sand was resuspended in 20 mL of ultrapure water, and reactors were pH adjusted to 11. Reactors were rotated end-over-end overnight before being sonicated for 15 minutes. Sand and liquid containing particles were separated from one another and both were air dried. Sand colors were lighter after detachment but still maintained a slight orange color indicating incomplete detachment. Minimal particle recovery was obtained. Two other pH values, 9 and 10, were also tested, but detachment was never as successful as reported by Sourush et al.[4] for goethite and pH 11 was used as it provided the best removal of particles from sand surfaces. Given this limited removal, sands were further digested by concentrated HCl and the supernatant from this digestion was serially diluted first in water followed by 1% nitric acid and analyzed by ICP-OES. For the LFe 36 column, ICP-OES results indicated that approximately 60% of the Fe remained on the sand surfaces following detachment.

S1.5 Example low temperature magnetic properties of mineral standards goethite, magnetite, hematite and lepidocrocite.

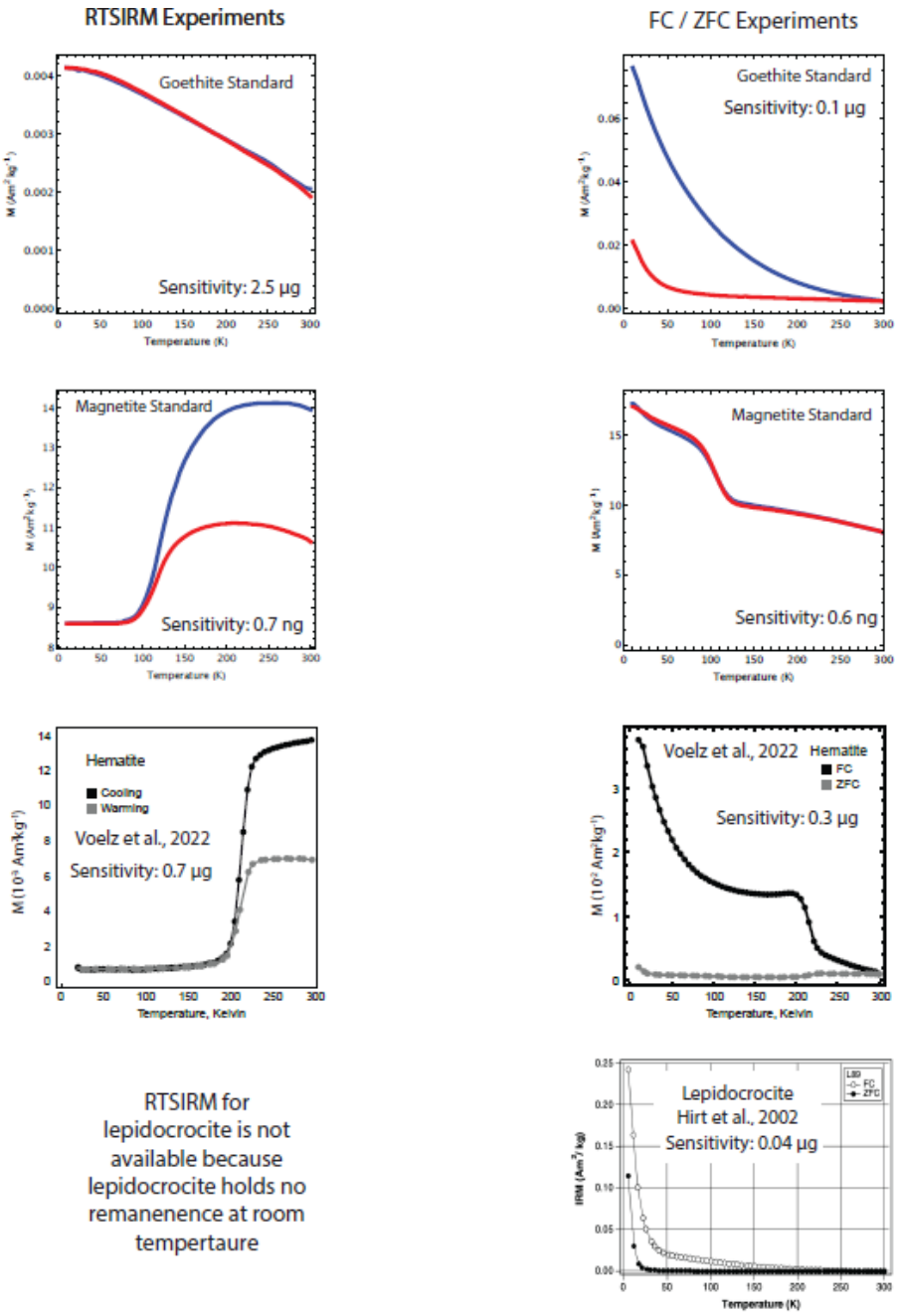

Figure S1. Room temperature isothermal remanent magnetization (RTSIRM; left panels) and field-cooled (FC) – zero-field-cooled (ZFC) measurements of mineral standards. Please note that scales are different from figure to figure. Sensitivities were calculated using an instrument sensitivity of 10^{-10} Am^2 and assume a required signal to noise of 100:1.[5,6]

S1.6 Calculation of particle mass and surface area

The average signal of Fe from the ICP-OES data for each wavelength measured was converted to mg Fe/g sand as follows. First the concentration of Fe in each ICP-OES sample was determined by:

$$[Fe]_{ICP-OES\ Sample} = (Signal_{Fe} - m_{Fe\ Calibration\ Curve})/b_{Fe\ Calibration\ Curve} \quad \text{(S5)}$$

where m and b are the slope and y-intercept from the linear least square regression of the external standardization calibration curve signals. Calibration curve standards are made in ppm so sample concentrations are calculated in ppm, as well.

The concentration of Fe that was digested from the sand sample was calculated by accounting for dilutions from the digestion liquid:

$$[Fe]_{Digested} = \frac{\frac{([Fe]_{ICP-OES\ Sample} * 11\ mL)}{1\ mL} * 10\ mL}{0.1\ mL} \quad \text{(S6)}$$

Volumes indicated come from dilutions needed during preparation of the samples. In this case, 0.1 mL was the volume of the digestion liquid diluted to 10 mL in ultrapure water, and 1 mL was the volume of the digestion dilution that is further diluted to 11 mL in 1% nitric acid.

For each sample, the concentration of Fe (in ppm) determined is multiplied by 0.002 L to determine the mg of Fe in the analyte. This value is used because ~1 g of sand was digested in 2 mL of conc. HCl.

The quantity of Fe (mg) in the analyte was then divided by the exact mass of sand digested (g) to determine the mg Fe/g sand in each sample. The average quantity of Fe in the unreacted sample (from the three wavelengths measured) was subtracted from the average quantity of Fe determined for the three different column zones to get the quantity of Fe determined from the post-reaction samples.

For each zone of the column, the mg Fe/g sand was multiplied by 23 to account for the total mass of sand used in the column and divided by 3 due to the division of the column into the three zones. These three values were added to get the total mass of Fe across the column.

For the lower coverage sample this value was 9.8 mg Fe in the column. For the higher coverage sample this value was 15.3 mg in the column

S1.7 Calculation of particle surface area:

Previous literature on the oxidative growth of goethite has shown that the {021}

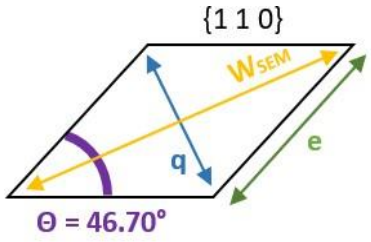

$$Area_{tip} = 2\left(\frac{w_{SEM} * q}{2}\right) \quad \text{(S7)}$$

$$q = 0.41 * w_{SEM} \quad \text{(S8)}$$

$$e = \frac{1}{2}\sqrt{(1 + 0.41^2) * {w_{SEM}}^2} \quad \text{(S9)}$$

crystal plane comprises a minor fraction of the accessible surface area for Fe(II) adsorption but is the primary facet of oxidative mineral growth.[7] If the tips of the particles are modeled by the cross-sectional rhombus of a Gt nanorod, as has been done in the previous work of Anschutz and Penn,[8] a portion of the available surface area can be approximated as the area of this rhombus: where w_{SEM} was approximated by sizing of particles observed in SEM micrographs using ImageJ software.

The rest of the particle can be considered to be composed of four rectangles, whose length comes from approximated measurements from sizing observed in SEM micrographs (l_{SEM}) and width comes from the edge of the aforementioned rhombus.

For the higher coverage sand, w_{SEM} and l_{SEM} were approximated to be 40 and 100 nm, respectively.

For the lower coverage sand, w_{SEM} and l_{SEM} were approximated to be 20 and 200 nm, respectively.

The mass of Fe localized in each particle was determined by considering the volume of the particle knowing the volume within the tip and the particle's length. This number when multiplied by the particle density, ρ, returns the mass per particle. Dividing this mass by the area of the sides of the particle, which was much greater than the area of the particle tips, the approximate surface area per gram of sand was found.

$$Volume_{Particle} = \left(\frac{w_{SEM} * q}{2}\right) * l_{SEM} \quad \text{(S10)}$$

$$Mass_{Particle} = Volume_{Particle} * \rho \quad \text{(S11)}$$

$$Surface\ Area_{Particle} = Mass_{Particle}/Area_{Side} \quad \text{(S12)}$$

The mass of Fe in the column was converted to mass of Gt using stoichiometric ratios. The surface area of goethite in the column was determined by multiplying the mass of goethite, in g, by the surface area of each particle.

$$Surface\ Area_{Column} = Surface\ Area_{Particle} * Gt_{Column} \quad \text{(S13)}$$

S2. Supplemental Results

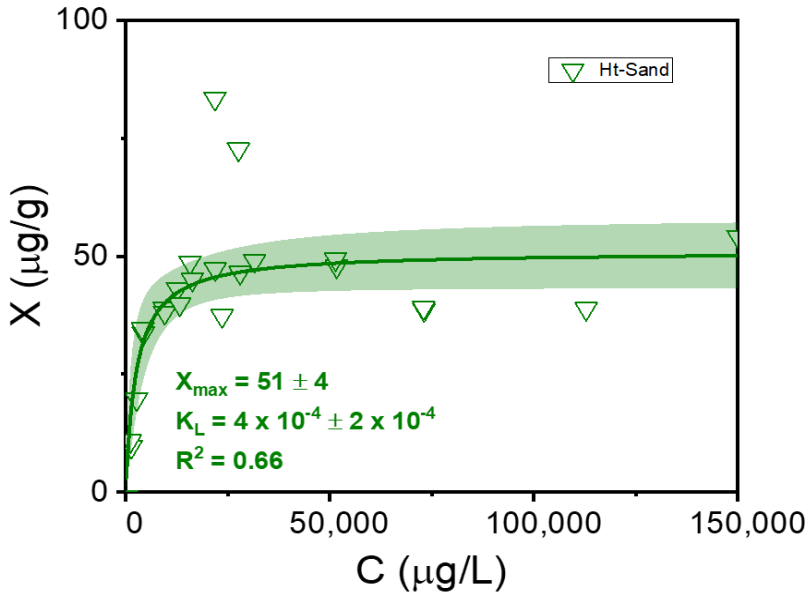

Figure S2. Sorption isotherms of Fe(II) on higher coverage hematite coated sand at pH 7 in 10 mM $NaHCO_3$ buffer. The solid line represents fitting with the Langmuir adsorption model and shaded error represents the 95% confidence band of the fit. Values are reported with the 95% confidence interval.

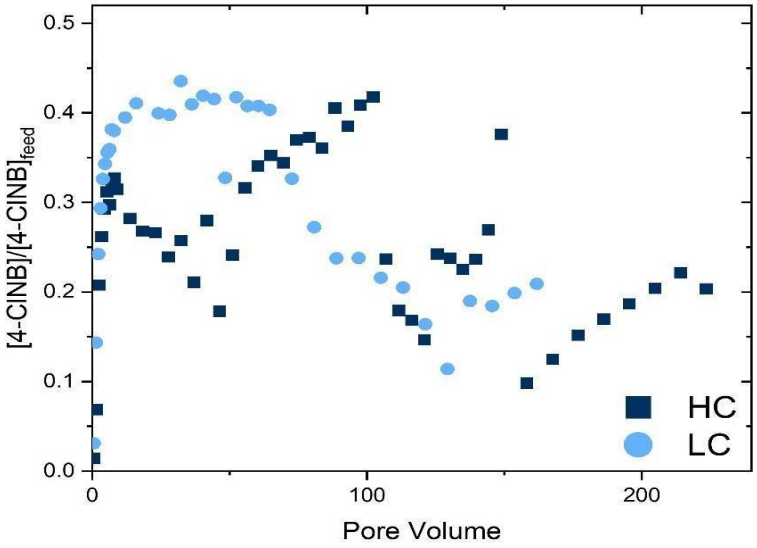

Figure S3. Concentration of 4-ClNB, relative to the feed concentration, for the lower coverage (LFe, light blue circles) and higher coverage (HFe, dark blue squares) hematite coated sands for reaction periods of 36 hours. Both columns approach a steady state where their relative 4-ClNB is at a similar level.

(a)

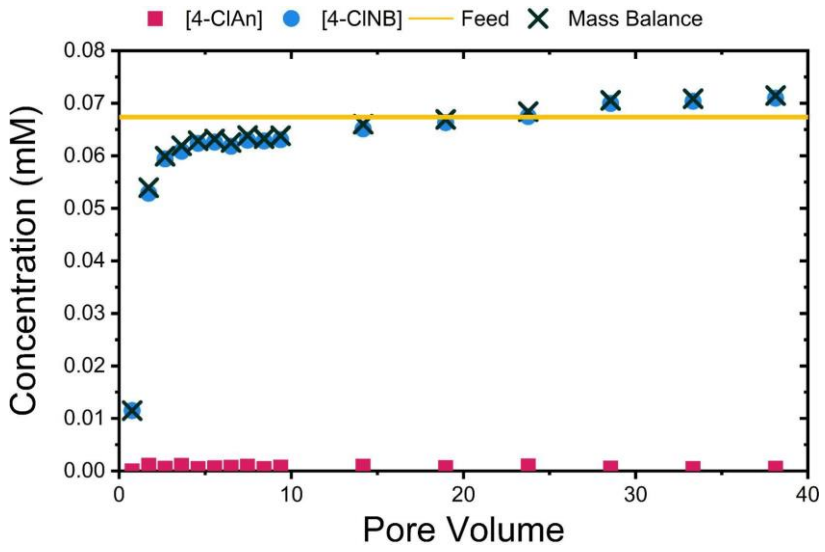

(b)

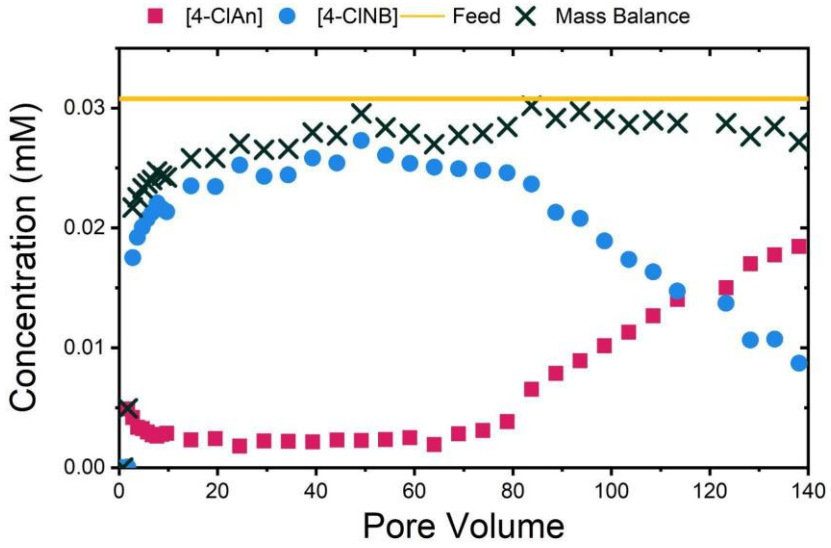

Figure S4: Concentration of 4-chloronitrobenzene (4-ClNB) from the influent (feed, yellow line) and effluent (red square), concentration of 4-chloroaniline (4-ClAn) in effluent (blue circle) and the summative mass balance of 4-ClNB and 4-ClAn (black X) for the lower surface coverage sand columns sacrificed after (a) 6 hours of reaction and (b) 21 hours of reaction.

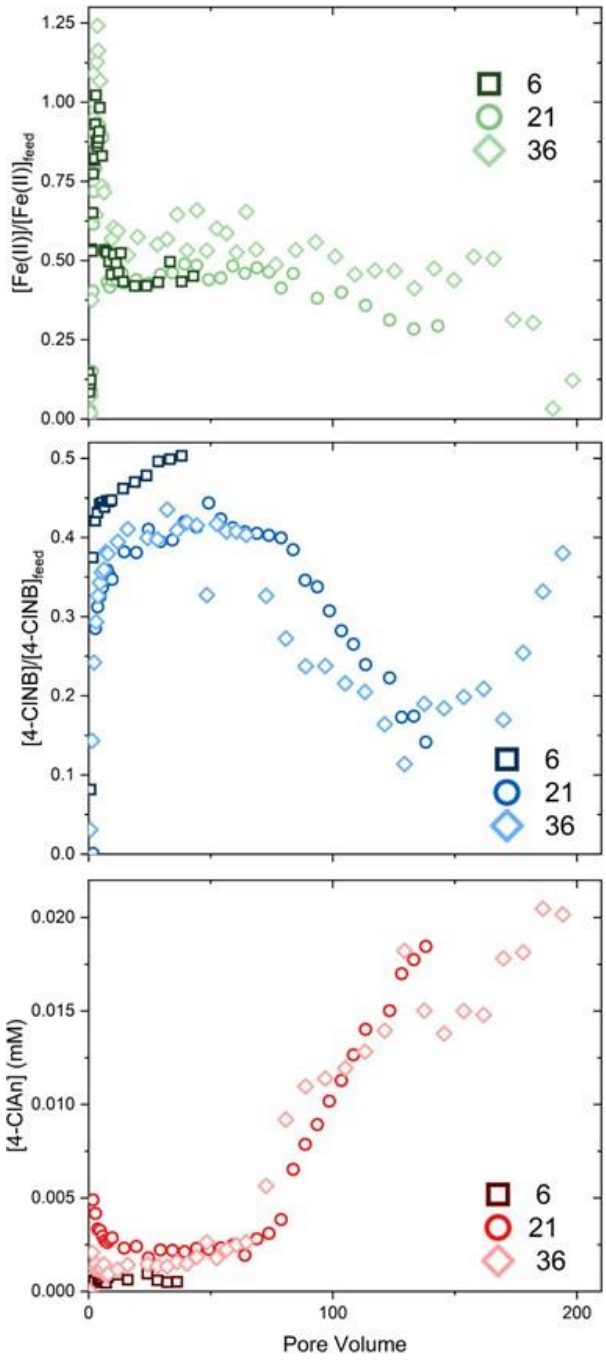

Figure S5: Relative concentration of Fe(II) (top, green), 4-ClNB (middle, blue), and absolute concentration of 4-ClAn (bottom, red) from the effluents of the LFe sand columns sacrificed after 6 hours of reaction (light shade, square), 21 hours of reaction (middle shade, circles), and 36 hours of reaction (dark shade, diamonds) demonstrating the overall reproducibility and similarity across the lower coverage columns.

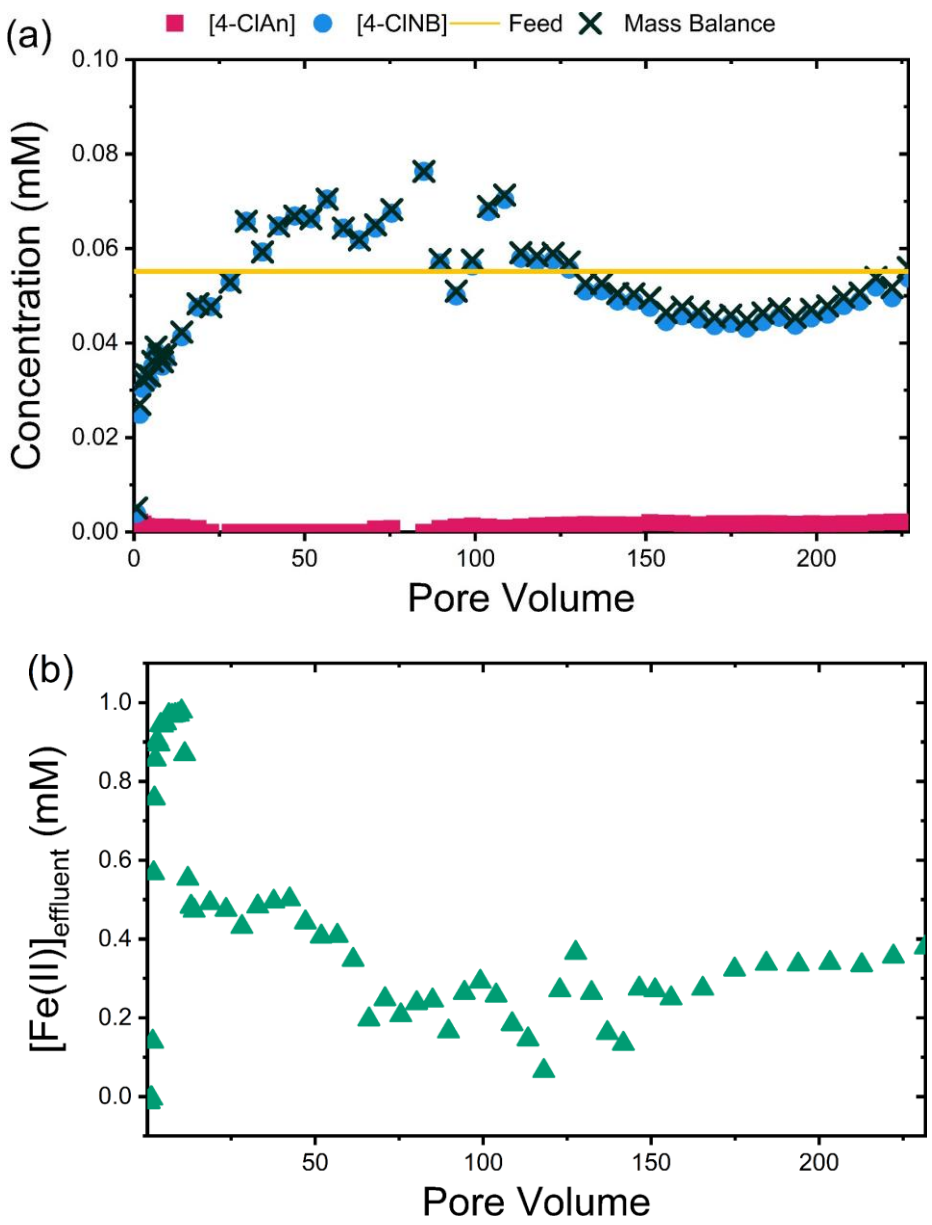

Figure S6: (a) Concentration of 4-chloronitrobenzene (4-ClNB) from the influent (feed, yellow line) and effluent (red square), concentration of 4-chloroaniline (4-ClAn) in effluent (blue circle) and the summative mass balance of 4-ClNB and 4-ClAn (black X) for the uncoated Ottawa sand standard during 36 hours of reaction. (b) Concentration of Fe(II) for the uncoated Ottawa sand standard during initial saturation period and following 36 hours of reaction. Variations in 4-ClNB and Fe(II) concentration resulted from flow discrepancies due to piston-pump.

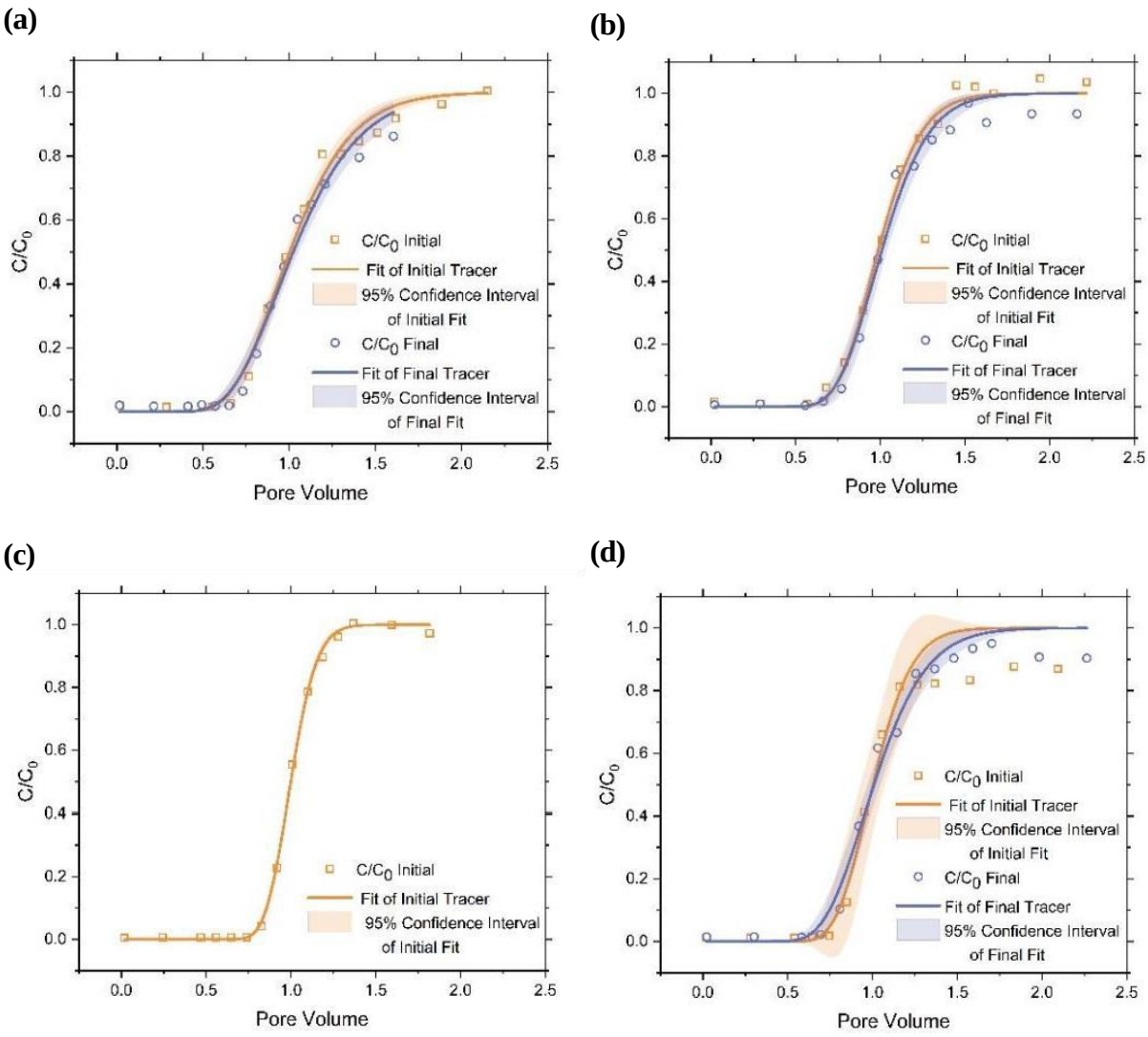

Figure S7: Breakthrough curves for the NaCl tracers of the lower coverage sand columns sacrificed after (a) 6 hours, (b) 21 hours, and (c) 36 hours of reaction, and the (d) higher coverage sand column sacrificed after 36 hours of reaction. In all cases, orange squares represent the initial measurement, and the purple circles represent the final measurement. Solid lines of the respective color indicate the fit and shaded regions of the respective color represent the fit's 95% confidence interval. The lower coverage sand column sacrificed after 36 hours of reaction was unable to be measured following reaction due to a piston pump mechanical issues which resulted in significantly dampened flow rates that impeded measurement and as such no final tracer measurement was performed.

For LFe 36, the post-reaction breakthrough curve could not be used due to a piston pump interruption, which resulted in significantly dampened flow rates. In all other cases, the Peclet number decreased after reaction, indicating an increased contribution from diffusive transport relative to the advective flow. The magnitude of the decrease in Peclet number increased with increasing reaction length and iron oxide formation. Porosity increased for LFe 6 and LFe 21, by 22 and 3 percentage points, respectively. In contrast, the porosity decreased for HFe sand by 5 percentage points. The increase in porosity observed for LFe 6 and LFe 21 likely arises from the loss of hematite during the initial rinsing stages. Given that LFe 6 undergoes little reaction, its post-reaction porosity reflects all of these losses. In contrast, LFe 21 has a smaller increase in porosity which implies that the iron oxide mineral mass is approximately equivalent after 21 hours of reaction, despite the initial losses due to rinsing. This conclusion is supported by the observation that the LFe 21 sand had a minimal increase in iron mass per gram of sand, as determined by ICP-OES (data not shown), relative to the unreacted and unrinsed sands. No trends were observed for variations in hydrodynamic dispersion coefficient.

Table S1. Summary of breakthrough curve fitting parameters before and after the reaction period for the hematite coated sand reaction columns for the lower coverage (LFe) and higher coverage (HFe) material, where numbers indicate length of reaction period (6 h, 12 h, and 36 h). Parameters include the Peclet number (Pe), percent porosity (ε) and the hydrodynamic dispersion coefficient(D). Dashes indicate data is unavailable.

ID	LFe 6		LFe 12		LFe 36		HFe 36	
Condition	Initial	Final	Initial	Final	Initial	Final	Initial	Final
Pe	26	22	50	43	138	--	64	35
ε (%)	63%	85%	61%	64%	75%	--	66%	61%t
D ($\times 10^2$, cm^2s^{-1})	3.7	3.2	2.0	2.2	0.6	--	1.5	2.9

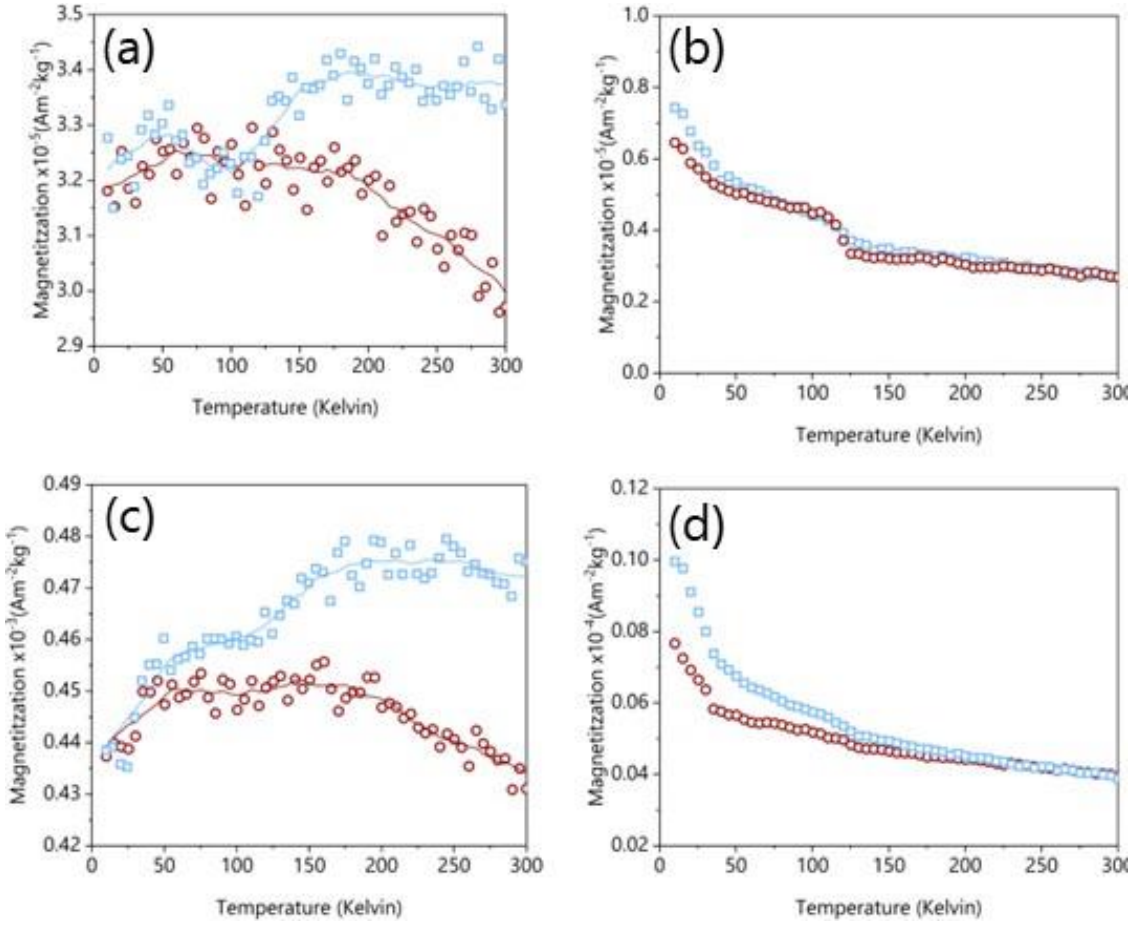

Figure S8: RTSIRM (left) data where blue squares (red circles) indicate cooling (warming), the lines are 9-point running averages, and FC/ZFC (right) data where blue squares (red circles) indicate data collected under FC (ZFC) conditions. Data was collected from acid-washed Ottawa sand (top: a, b) and unreacted LFe hematite coated sand (bottom: c,d). Figure were interpreted in comparison to Figure S1.

Ferrihydrite would be exceedingly difficult to see because its magnetization per mass is orders of magnitude less than that of hematite and goethite. When magnetic measurements have been used to examine ferrihydrite, it is typically for synthetic, monomineralic samples of ferrihydrite. Lepidocrocite does have characteristic low temperature magnetic behaviors, but it is unlikely to be present in these samples. If present, we would see lepidocrocite in the FC/ZFC data as the mineral goes from being an antiferromagnet to a paramagnet at ~50K (Hirt et al., 2002 in Figure S1). We would not observe lepidocrocite in RTSIRM experiments because it holds no permanent magnetization at room temperature. While we cannot completely rule out the possibility that lepidocrocite is present in the FC/ZFC data of the top specimen (Figure 4d), it is not

present in the middle or bottom portions of the column. Instead, goethite is increasingly present in the middle and bottom portions of the column, as seen by the increasing difference in the FC and ZFC data and the increasing negative slope of the RTSIRM data. Further, the presence of lepidocrocite in the top portion of the column is also unlikely because if it were present, we would expect to see a more prominent loss in remanence at during warming to 50K.

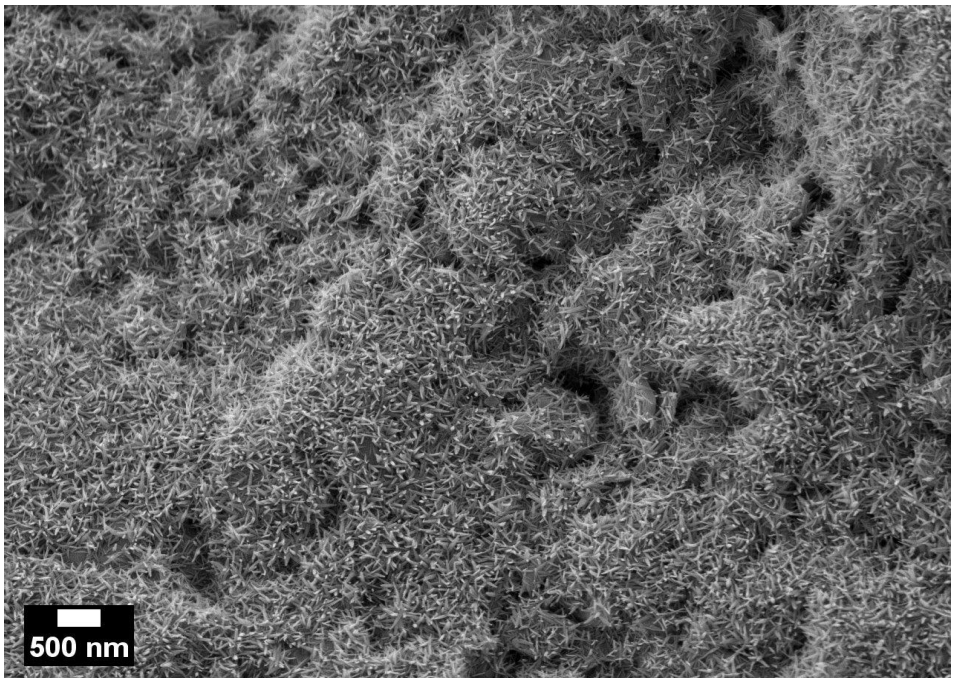

Figure S9: Large field of view SEM micrograph of post-reaction hematite-coated sand grains from the bottom of the LFe 36 column.

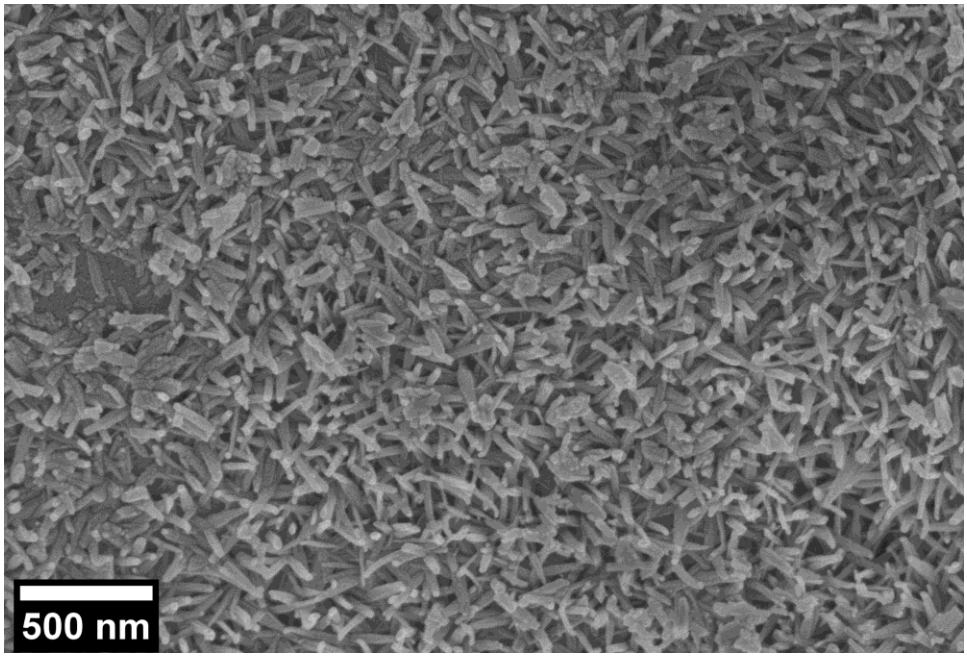

Figure S10: Large field of view SEM micrograph of post-reaction hematite-coated sand grains from the middle of the LFe 36 column.

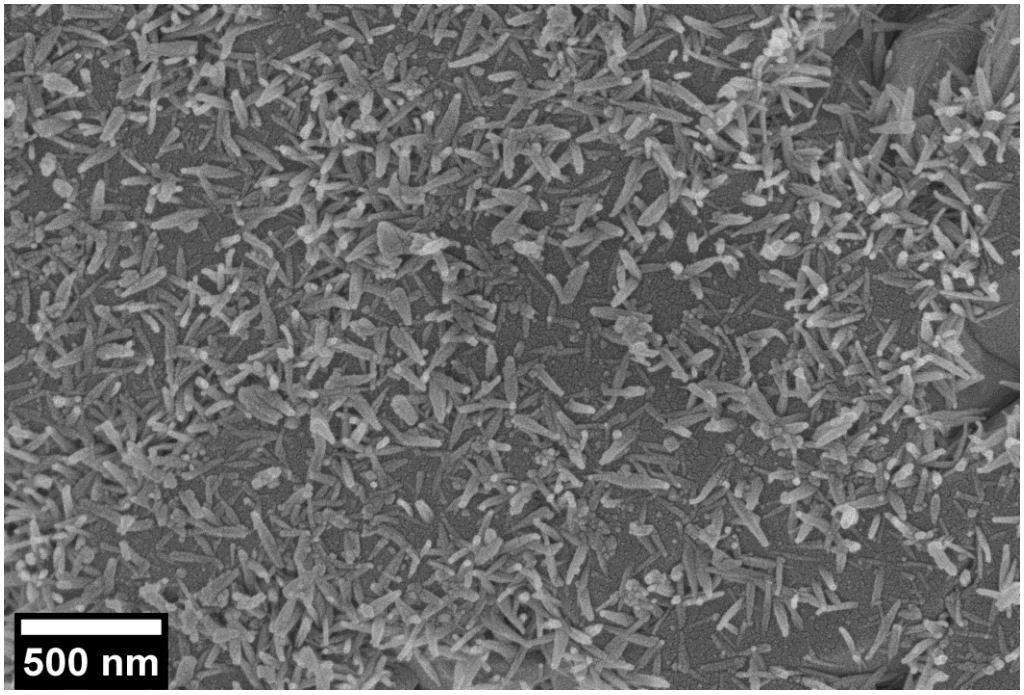

Figure S11: Large field of view SEM micrograph of post-reaction hematite-coated sand grains from the top of the LFe 36 column.

S3. References

(1) van Genuchten, M. T.; Parker, J. C. Boundary Conditions for Displacement Experiments through Short Laboratory Soil Columns. *Soil Sci. Soc. Am. J.* **1984**, *48* (4), 703–708. https://doi.org/10.2136/sssaj1984.03615995004800040002x.

(2) Voelz, J. L.; Arnold, W. A.; Penn, R. L. Redox-Induced Nucleation and Growth of Goethite on Synthetic Hematite Nanoparticles. *Am. Mineral.* **2018**, *103* (7), 1021–1029. https://doi.org/10.2138/am-2018-6342.

(3) Larese-Casanova, P.; Scherer, M. M. Fe(II) Sorption on Hematite: New Insights Based on Spectroscopic Measurements. *Environ. Sci. Technol.* **2007**, *41* (2), 471–477. https://doi.org/10.1021/es0617035.

(4) Soroush, A.; Penn, R. L.; Arnold, W. A. Anisotropic Oxidative Growth of Goethite-Coated Sand Particles in Column Reactors during 4-Chloronitrobenzene Reduction by Fe(II)/Goethite. *Environ. Sci. Nano* **2022**, *9*, 275-288.. https://doi.org/10.1039/D1EN00788B.

(5) Hirt, A. M.; Lanci, L.; Dobson, J.; Weidler, P.; Gehring, A. U. Low-Temperature Magnetic Properties of Lepidocrocite. *J. Geophys. Res. Solid Earth* **2002**, *107* (B1), EPM 5-1-EPM 5-9. https://doi.org/10.1029/2001JB000242.

(6) Voelz, J. L.; Hobart, K. K.; Stahovich, K. A.; Ziebol, H. E.; Harper, N. A.; Feinberg, J. M.; Arnold, W. A.; Penn, R. L. Organic Matter Inhibits Redox Activity and Impacts Heterogeneous Growth of Iron (Oxyhydr)Oxides on Nano-Hematite. *ACS Earth Space Chem.* **2022,** *6*, 847-860. https://doi.org/10.1021/acsearthspacechem.1c00419.

(7) Strehlau, J. H.; Stemig, M. S.; Penn, R. L.; Arnold, W. A. Facet-Dependent Oxidative Goethite Growth As a Function of Aqueous Solution Conditions. *Environ. Sci. Technol.* **2016**, *50* (19), 10406–10412. https://doi.org/10.1021/acs.est.6b02436.

(8) Anschutz, A. J.; Penn, R. L. Reduction of Crystalline Iron(III) Oxyhydroxides Using Hydroquinone: Influence of Phase and Particle Size. *Geochem. Trans.* **2005**, *6* (3), 60. https://doi.org/10.1186/1467-4866-6-60.